






FOXD2-AS1 is modulated by METTL3 with the assistance of YTHDF1 to affect proliferation and apoptosis in esophageal cancer

ZI JIN WANG 
XING CHEN LIU 
ZHEN GYA GAO 
WO DA SHI* 
WEN CAI WANG* 

Department of Cardiothoracic Surgery, Affiliated Hospital 6 of Nantong University
The Yancheng School of Clinical Medicine of Nanjing Medical University, Yancheng Third People's Hospital, Yancheng Jiangsu, 224000 China

ABSTRACT

This study aims to investigate the regulatory mechanisms of METTL3, YTHDF1, and the long non-coding RNA FOXD2-AS1 in the proliferation and apoptosis of esophageal cancer, with the goal of providing a basis for molecular diagnosis and targeted therapies. Gene expression was evaluated using qRT-PCR (METTL3/14) and Western blot analysis. The Cell Counting Kit-8 (CCK-8) assay, flow cytometry, and Transwell assay were employed to assess cell proliferation and apoptosis. The EpiQuik m6A RNA Methylation Quantification Kit was utilized to quantify total m6A levels. The interaction between YTHDF1, FOXD2-AS1, and METTL3 was confirmed using RNA Binding Protein Immunoprecipitation (RIP), Co-Immunoprecipitation (CO-IP), and RNA pull-down assays. Methylated RNA Immunoprecipitation (MeRIP) was employed to assess the m6A modification levels of FOXD2-AS1. Tissue samples from animal models were analyzed via Hematoxylin-eosin staining (HE) staining and immunohistochemistry to assess METTL3 expression.

The expression of *METTL3* was up-regulated in esophageal cancer tissues and cells. Flow cytometry and CCK-8 detection showed that silencing *METTL3* could inhibit the proliferation of esophageal cancer cells but accelerate their apoptosis. MeRIP-qPCR and Prediction of m6A-modified sites indicated that *METTL3* regulated the m6A modification of FOXD2-AS1. *In vitro* and *in vivo* experiments showed that YTHDF1 binds to METTL3 and regulates the m6A modification of FOXD2-AS1 to affect esophageal cancer. Our results indicate that METTL3 regulates FOXD2-AS1 in an m6A-dependent manner through its interaction with YTHDF1, thereby influencing EC proliferation and apoptosis. This suggests a potential therapeutic target for the treatment of esophageal cancer.

Keywords: esophageal cancer, FOXD2-AS1, METTL3, YTHDF1

Accepted March 19, 2025
Published online March 20, 2025

INTRODUCTION

Esophageal cancer (EC), which includes esophageal squamous cell carcinoma (ESCC; 90 %) and esophageal adenocarcinoma (EAC), is a major contributor to cancer-related mortality, primarily due to the advanced stage at diagnosis and limited treatment efficacy (1, 2).

* Correspondence; e-mail: wangwencai1949@sina.com

Its aggressive nature, coupled with an increasing incidence and poor prognosis, underscores the urgent need for enhanced treatment strategies (3). Despite the introduction of novel therapeutic approaches such as immunotherapy, chemoradiotherapy, and molecular therapy (5–7), the 5-year survival rate for advanced EC remains dismal (4). Unfortunately, these approaches have yielded unsatisfactory outcomes, particularly in regions with a high incidence of EC, such as China (8). Therefore, novel therapies targeting the oncogenesis of EC are urgently needed.

Long non-coding RNAs (lncRNAs) have recently emerged as pivotal regulators in the initiation and progression of various tumors (9). These non-coding RNA transcripts, which exceed 200 nucleotides in length, regulate mRNA transcription and translation, protein stability, epigenetic modifications, and other critical biological processes (10, 11). FOXD2-AS1, previously associated with multiple tumor types, has also been implicated in the oncogenesis of EC. FOXD2-AS1, in collaboration with MACC1-AS1, mediates cisplatin resistance in ESCC cells through NSD2 induction (15). Overexpression of FOXD2-AS1 is associated with cisplatin resistance in ESCC by targeting miR-195 and modulating the Akt/mTOR signaling pathway (16). Our previous research demonstrated that FOXD2-AS1 promotes proliferation and invasion through the miR-145-5p/CDK6 axis in EC (17). This study aims to elucidate the upstream mechanisms regulating the role of FOXD2-AS1 in EC.

*N*⁶-methyladenosine (m6A) RNA modification is the most prevalent RNA modification in eukaryotes and is regulated by three classes of enzymes: m6A methyltransferases (METTL3/14), m6A demethylases (ALKBH5 and FTO), and m6A reading enzymes (YTHDF1/2/3) (18). Recent studies have revealed the presence of m6A RNA modifications in various non-coding RNAs, including miRNAs, lncRNAs, and circRNAs (19). METTL3, an m6A methyltransferase, is an S-adenosylmethionine (SAM)-binding protein highly conserved across eukaryotes (20). The m6A methyltransferase complex plays a crucial role in RNA methylation modification. The core of this complex consists of a heterodimer composed of methyltransferase-like protein 3 (METTL3) and methyltransferase-like protein 14 (METTL14) (21). Among these components, METTL3 is the only catalytically active element, responsible for transferring methyl groups to the *N*⁶ position of adenine nucleotides in RNA. In contrast, METTL14 contributes to the structural stabilization of METTL3, facilitating both the maintenance of the complex's integrity and the recognition of RNA substrates (22). YTH N⁶-methyladenosine RNA-binding protein 1 (YTHDF1) acts as a key reader enzyme of m6A RNA modifications (23), and there is increasing evidence supporting the role of m6A methylation in various cancers. In breast cancer, METTL3 has been shown to regulate MALAT1 expression, thereby modulating the E2F1/AGR2 axis and promoting resistance to adriamycin (24). YTHDF1 has also been implicated in driving breast cancer by enhancing FOXM1 translation in an m6A-dependent manner (25). However, the impact of m6A RNA modification on the initiation and progression of esophageal cancer (EC) through the regulation of lncRNA expression remains to be explored.

In this study, we first observed elevated METTL3 expression in esophageal cancer (EC) tissues and cells. Subsequently, loss-of-function experiments were performed to evaluate cell proliferation and apoptosis. Mechanistic investigations examined the molecular interplay between METTL3 and FOXD2-AS1, involving YTHDF1, in EC cells. Furthermore, *in vivo* experiments were conducted to assess the functional significance of the METTL3/FOXD2-AS1 axis in EC animal models.

EXPERIMENTAL

Bioinformatics prediction

The Encyclopedia of RNA Interactomes (ENCORI, <https://starbase.sysu.edu.cn/index.php>) (26) and The University of ALabama at Birmingham CANcer (UALCAN, <https://ualcan.path.uab.edu/index.html>) databases were used to analyze the expression of *METTL3* and *METTL14* in EC tissues and normal tissues (27–28). The sequence-based RNA adenosine methylation site predictor (SRAMP, <http://www.cuilab.cn/sramp>) (29–30) was used to analyze the m6A-modified sites in *FOXD2-AS1*. The correlation between *FOXD2-AS1* and *YTHDF1* in esophageal cancer was analyzed using the Gene Expression Profiling Interactive Analysis (GEPIA, <http://gepia.cancer-pku.cn/>) (31) database. All the above results were obtained on the TCGA-ESCA dataset (32).

Collection of clinical tissues

Clinical samples of esophageal cancerous and adjacent non-cancerous tissues were collected from 10 patients who underwent treatment at the Sixth Affiliated Hospital of Nantong University. The samples were immediately frozen in liquid nitrogen for preservation. None of the patients had received interventional therapy or systemic chemotherapy prior to surgery, and informed consent was obtained from either the patients or their legal guardians. All experiments were approved by the Ethics Committee of the Sixth Affiliated Hospital of Nantong University (2020-081).

Cell culture

Human normal esophageal epithelial cells (T-HEECs) and esophageal cancer (EC) cell lines (Eca-109 and TE-1) were obtained from the Cell Resource Center of the Shanghai Academy of Sciences and cultured in DMEM supplemented with 10 % fetal bovine serum (FBS) and 1 % penicillin-streptomycin. Cells were cultured in a humidified incubator at 37 °C with 5 % CO₂.

qRT-PCR analysis

Total RNA was isolated from tissues and cells using TRIzol reagent (Invitrogen, USA), followed by complementary DNA (cDNA) synthesis using the PrimeScript RT reagent kit (TaKaRa, China). Quantitative PCR (qPCR) was performed using SYBR Green (Vazyme Biotech, China) on a GeneAmp 7500 system (Applied Biosystems, Thermo Fisher, USA). RNA expression levels were quantified using the 2^{- $\Delta\Delta C_t$} method (33), with GAPDH as the internal control. Primers were designed using the NCBI website (<https://www.ncbi.nlm.nih.gov/tools/primer-blast/>) (34). The amplification process was set as follows: the predenaturation stage lasted at 95 °C for 300 s, and then entered a cycling reaction. Each cycle included denaturation at 95 °C for 10 s and annealing at 60 °C for 30 s, a total of 45 cycles. The primer sequences used were as follows: *METTL3*, forward 5'-AAGCTGCACTTCAGACGAAT-3' and reverse 5'-GGAATCACCTCCGACACTC-3'; *METTL14*, forward 5'-GAACACAGAGCTTAATCCCA-3' and reverse 5'-TGTCAGCTAAACCTACATCCCTG-3'; *FOXD2-AS1*, forward 5'-TGGACCTAGCTGCAGCTCCA-3' and reverse 5'-AGTTGAAGGTGCACACACTG-3';

YTHDF1, forward 5'-ATGTCGGCCACCAGCGTGGACA-3' and reverse 5'-TCATTGTT-TGTTTCGACTCTGC-3'; YTHDF2, forward 5'-CATGAATGGGAAGGGTCCCG-3' and reverse 5'-GACGAATGTGTCCGAGTTGG-3'; YTHDF3, forward 5'-TGTTGTGGACTATA-ATGCGTATGC-3' and reverse 5'-AAGCGAATATGCCGTAATTGGTTA-3'; GAPDH, forward 5'-GGAGCGAGATCCCTCCAAAAT-3' and reverse 5'-GGCTGTTGTCATACTTCTCATGG-3'.

Cell transfection

To silence the expression of FOXD2-AS1, siRNAs targeting FOXD2-AS1 (siFOXD2-AS1-1 and siFOXD2-AS1-2) were used. To reduce METTL3 expression, shMETTL3-1 and shMETTL3-2 were applied. As for the construction of the shRNA expression vector, after designing synthetic primers based on *METTL3* gene transcript, the transformants were screened by colony PCR and verified by sequencing. For modulating YTHDF1 expression, siYTHDF1 and pc-YTHDF1 were employed. In control experiments, siNC or pc-DNA3.1 served as negative controls. These plasmid transfections from GenePharma were carried out in Eca-109 and TE-1 cells using Lipofectamine 2000 reagent (Invitrogen). The sequences were as follows:

siFOXD2-AS1-1, sense: 5'-GGGCAAAGUUCGAGAGUGATT-3' and anti-sense: 5'-UCACUCUCGAACUUUGCCCTT-3'; siFOXD2-AS1-2, sense: 5'-GGACUGGUUCU-GAGACAAATT-3' and anti-sense: 5'-UUUGU -CUCAGAACCAGUCCTT-3'(8); pc-DNA3.1: F-CTAGAGAACCCACTGCTTAC R-TAGAAGGCACAGTCGAGG. ShMETTL3-1: CcggGCC AAGGAACAATCCATTGTTCTCGAGAACAAATGGATTGTTCCCTGGCTTTTTTg; shMETTL3-2: CcggCGTCAGTATCTTGGGCAAGTTCTCGAGAACTTGCCCAAGATACTG ACGTTTTTTg; shNC: CcggGCTGCACTTCAGACGAATTATCTCGAGATAATTCGCTCGA AGTGCAGCTTTTTTg.

Cell counting kit 8 (CCK-8) assay

1×10^4 cells were seeded into each well of a 96-well plate. Subsequently, 10 μ L of CCK-8 (Dojindo, China) reagent was introduced into each well, and cells were cultured using serum-free medium (12309019, Thermo Fisher). This process was carried out at 24, 48, and 72 hours. After a 2-hour incubation, the absorbance at 450 nm in each well was measured using a microplate reader (BioTex, USA).

EdU incorporation assay

Cells were incubated with 10 mM EdU for 2 hours, then fixed with 4 % paraformaldehyde, permeabilized with 0.3 % Triton X-100, and stained with Apollo fluorescent dye (Sigma-Aldrich, China). Nuclei were stained with 5 mg mL⁻¹ 4',6-diamidino-2-phenylindole (DAPI) (D9542, Sigma-Aldrich) for 10 minutes. The number of EdU-positive cells in five random fields was counted under the Zeiss UV LSM 510 confocal microscope. All experimental procedures were performed according to the instructions of the kit (C0078S, Beyotime, China).

Flow cytometry

To assess the apoptosis ability of tumor cells, the PE Annexin V Apoptosis Detection Kit I (BD Pharmingen) was used. Cells were harvested, resuspended in $1 \times$ binding buffer,

and collected in a 10 mL centrifuge tube. Incubation with 5- μ L PE Annexin V and 5- μ L 7-AAD was conducted for 15 min. Apoptotic cells were assessed using a FACS Calibur flow cytometer (BD Bioscience, USA).

Western blotting

To assess the protein expression of METTL3, METTL14, YTHDF1, Bax, c-caspase-3, t-caspase-3, PCNA, and Ki-67 in Esophageal cancer cells and tissues, protein extraction was performed using RIPA lysis buffer (Beyotime). The protein concentration was determined using a BCA Protein assay kit (Beyotime). Subsequently, the proteins were separated on SDS-PAGE and transferred onto PVDF membranes. Blocking was achieved using 5 % skimmed milk (P0216, Beyotime). Primary antibodies against METTL3 (1:1000; 67733-1-IG, Proteintech, China) METTL14 (1:1000; F1391, Selleck, China) YTHDF1 (1:500; 66745-1-IG, Proteintech), Bax (1:1000; Cat. #2772T, CST, China), c-caspase-3 (1:1000; Cat. #9661T, CST), t-caspase-3 (1:1000; 82202-1-RR, Proteintech), PCNA (1:500; Cat. #13110T, CST), Ki-67 (1:700; ab15580, Abcam, China), and GAPDH (1:1000; sc-32233, Santa Cruz Biotechnology, USA) were incubated overnight in a 5 % milk dilution followed by incubation with HRP-labeled goat anti-rabbit IgG. The blots were then visualized using chemiluminescence (HRP Substrate) and captured with an AlphaView analysis system (ProteinSimple) (FluorChem R, USA). GAPDH was used as a referent protein for calculating protein expression, and protein band quantification was performed using ImageJ software (v1.8.0) (35).

Quantification of m6A RNA methylation

Total RNA was extracted from cells following the manufacturer's instructions, using the TRIzol reagent (Thermo Fisher). m6A RNA methylation levels were quantified using the EpiQuik m6A RNA Methylation Quantification Kit (Colorimetric; Epigentek) and measured at an absorbance of 450 nm.

RNA stability assays

Cells were seeded in 6-well plates and transfected with either shNC or shMETTL3. Following transfection, cells were treated with actinomycin D (CST, 5 μ g mL⁻¹) for 0, 4, and 8 hours. RNA was then extracted to evaluate the levels of the target RNA via real-time PCR.

Co-IP

To investigate the interaction between METTL3 and YTHDF1 proteins, we performed a Co-IP (co-immunoprecipitation) assay. We first constructed the METTL3-Myc[®] expression vector by fusing the METTL3 coding sequence with the pc-AMBIA1300-35S-Myc-rbcsE9 vector (NM_019852.5) (F- CGCAAATGGGCGGTAGGCGTG; R-CATAGCGTA-AAAGGAGCAACA). Similarly, we generated the YTHDF1-GFP[®] expression vector by amplifying and fusing the coding sequence of YTHDF1 with the pc-AMBIA1300-35S-GFP-rbcsE9 vector (NM_017798.4) (F- CGCAAATGGGCGGTAGGCGTG; R- GACACGCTG-AACTTGTGGC). Subsequently, these expression vectors were transfected into the appropriate cells. The cells were lysed under non-denaturing conditions, and the resulting lysate

was collected. The lysate was then incubated with either anti-GFP (P2132, Beyotime) or anti-MYC (P2118, Beyotime) beads at 4 °C for 4 hours. Following incubation, we carried out five washes using an extraction buffer. Subsequently, we eluted the proteins from the magnetic beads by boiling the samples in the SDS sample buffer for 10 minutes. Afterward, we isolated the proteins *via* SDS-PAGE electrophoresis and performed Western Blots to detect the presence of the proteins.

RNA immunoprecipitation (RIP)

To validate the interaction between *FOXD2-AS1* and *YTHDF1*, *YTHDF2*, or *YTHDF3*, we performed RNA immunoprecipitation (RIP) using the EZMagna RIP Kit (Millipore, USA). After washing and scraping the cells with PBS, they were centrifuged and resuspended in complete RIP lysis buffer. Antibodies (IgG, *YTHDF1*, *YTHDF2*, and *YTHDF3*) were pre-incubated with Protein A/G magnetic beads in an immunoprecipitation buffer. The cell lysates were then incubated with the antibody-bead complexes overnight at 4 °C. The RNA eluted from the beads was precipitated with ethanol, dissolved in RNase-free water, and analyzed by qPCR to assess *FOXD2-AS1* expression. The antibodies used were IgG (10284-1-AP, Proteintech), *YTHDF1* (#86463, CST), *YTHDF2* (24744-1-AP, Proteintech), and *YTHDF3* (#242065, CST).

M6A MeRIP qPCR

To quantify the m6A methylation level of *FOXD2-AS1*, we performed m6A methylated RNA immunoprecipitation (MeRIP) using an m6A-specific antibody and the Magna m6A MeRIP Kit (Millipore). Following cell treatment (transfection with shNC, shMETTL3-1, and shMETTL3-2), RNA was extracted from Eca-109 and TE-1 cells using the Trizol reagent (Invitrogen). After fragmenting the RNA, immunoprecipitation was carried out using m6A or IgG antibodies in 1 ml of buffer supplemented with ribonuclease inhibitors. Following washing, protein A/G magnetic beads were added to the mixture and incubated for 2 hours at 4 °C. The m6A RNA was then eluted using N6-methyladenosine-5'-monophosphate sodium salt at 4 °C for 1 hour, followed by RNA purification and qPCR analysis to investigate the regulation of *FOXD2-AS1* by *METTL3*.

RNA pull-down assay

To investigate the binding interaction between *YTHDF1* and *FOXD2-AS1*, we performed an RNA pull-down assay. A biotinylated *FOXD2-AS1* probe was designed and synthesized by RiboBio. The cells were transfected with the probe and treated for 2 days. Subsequently, the cells were washed, lysed, and incubated at 4 °C with Dynabeads™ M-280 Streptavidin magnetic beads (Invitrogen). The precipitated proteins were then purified using TRIzol for western blot analysis.

Animal models

The procedures involving animal assays were conducted following approval from the Ethical Committee of Affiliated Hospital 6 of Nantong University (XMLL-2021-808). A total of 24 BALB/c nude mice, aged 4–6 weeks and weighing 18–20 grams, were subcutaneously injected with cells transfected with various constructs, including a blank vector (NC

group), shMETTL3-1 (METTL3 KD group), pc-FOXD2-AS1 (FOXD2-AS1 OE group), and shMETTL3-1+pc-FOXD2-AS1 (METTL3 KD+FOXD2-AS1 OE group). The injections were administered to the right flank of the mice. Over a 28-day period, tumor volume measurements were taken every 3 days, and the recorded data were calculated using the formula $(\text{length} \times \text{width}^2)/2$. Additionally, upon sacrificing the mice, the tumors were excised, and their weights were measured.

FISH

Specific FISH probes for *FOXD2-AS1* were designed and synthesized by Servicebio (China). Hybridization was performed in mouse tumor tissue, as previously reported (36). All images were analyzed using a fluorescence microscope. The FISH probe sequence for *FOXD2-AS1* was as follows: 5'-TAAAATTAGAGAAATCTGCGGGCGTAGTCCCCAAGC-3'.

Immunohistochemistry (IHC)

Formalin-fixed tissue samples were sectioned into 5- μm slices. Subsequently, dewaxing, hydration, and heat-induced epitope retrieval were performed. The sections were treated with a primary antibody against METTL3 (1:1000; 67733-1-IG, Proteintech), Ki-67 (1:1000; ab15580, Abcam) followed by incubation with secondary antibodies (1:3000; ab205719, Abcam) and peroxidase-conjugated streptavidin. A 3,3'-diaminobenzidine tetrahydrochloride (DAB) solution (36201ES03, Yeasen, China) was applied for 5 minutes, and counterstaining was carried out with hematoxylin. The stained sections were then observed under a light microscope. For protein quantification of METTL3: the number of METTL3-positive cells in five random areas was counted at 40 \times magnification, and the average value was the number of METTL3-positive cells in that section.

Hematoxylin and eosin (HE) staining

Paraffin-embedded tissue sections were subjected to a 30-minute roasting process (70 $^{\circ}\text{C}$), followed by dewaxing and hydration. The cell nuclei were stained with hematoxylin solution (Biosharp, China), and the cytoplasm was stained with eosin solution (Biosharp). After the sections were allowed to dry, they were preserved using a neutral resin.

Statistical analysis

All experiments were performed in triplicate, and statistical significance was determined at a level of $p < 0.05$. Statistical analyses were conducted using SPSS 21.0 software (IBM). Differences were assessed using either the student's *t*-test or one-way ANOVA (Tukey's post hoc test). Additionally, a ROC curve was generated to assess the diagnostic value of FOXD2-AS1 expression for EC patients.

RESULTS AND DISCUSSION

METTL3 was upregulated in EC tissues and cells

The ENCORI database analysis revealed a significant increase in *METTL3* expression in EC tissues compared to normal tissues, with no significant change in *METTL14* expression (Fig. 1a). Furthermore, UALCAN database analysis showed that *METTL3* expression

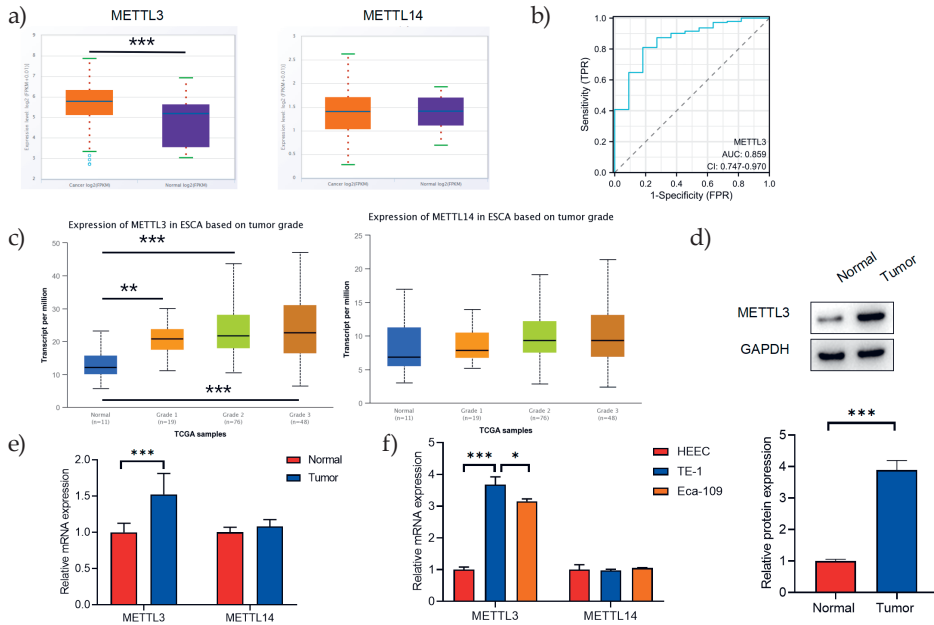


Fig. 1. METTL3 expression was upregulated in EC tissues and cells: a) ENCORI analysis of elevated *METTL3* expression and unaltered *METTL14* expression in EC tissues compared to normal tissues; b) ROC curve analysis evaluating the potential diagnostic value of *METTL3* expression levels in esophageal cancer; c) UALCAN database analysis of *METTL3* and *METTL14* expression based on tumor grade; d) WB analysis of *METTL3* expression in the samples; e) qRT-PCR analysis showing the expression levels of *METTL3* and *METTL14* in 10 matched EC and non-tumor tissues; f) qRT-PCR analysis of *METTL3* and *METTL14* expression in HEEC, Eca-109, and TE-1 cells. * $p < 0.05$, ** $p < 0.01$, *** $p < 0.001$.

increased with tumor grade, while *METTL14* expression remained relatively unchanged (Fig. 1c). The receiver operating characteristic (ROC) curve showed that the expression level of *METTL3* in esophageal cancer had potential diagnostic value (Fig. 1b) (32). The expression of *METTL3* protein in tissues was confirmed through WB, revealing a significant upregulation of *METTL3* in cancerous tissues compared to normal tissues (Fig. 1d) ($p < 0.001$). To validate these predictions, *METTL3* and *METTL14* mRNA levels were assessed in tissues and cells using qRT-PCR. In comparison to normal tissues, only *METTL3* showed a significant upregulation in cancerous tissues (Fig. 1e) ($p < 0.001$). High levels of *METTL3* were observed in Eca-109 and TE-1 cells compared to HEEC (Fig. 1f) ($p < 0.001$, $p = 0.023$). In summary, *METTL3* is significantly overexpressed in EC tissues and cells.

METTL3 silencing suppressed proliferation and accelerated apoptosis of EC cells

To investigate the functional role of *METTL3* in EC, qRT-PCR results confirmed the successful silencing of *METTL3* (Fig. 2a) (Eca-109: shNC vs. sh*METTL3*-1, $p < 0.001$; shNC vs. sh*METTL3*-2, $p < 0.001$) (TE-1: shNC vs. sh*METTL3*-1, $p < 0.001$; shNC vs. sh*METTL3*-2, $p < 0.001$). Following *METTL3* knockdown, the total m6A level was also reduced (Fig. 2b)

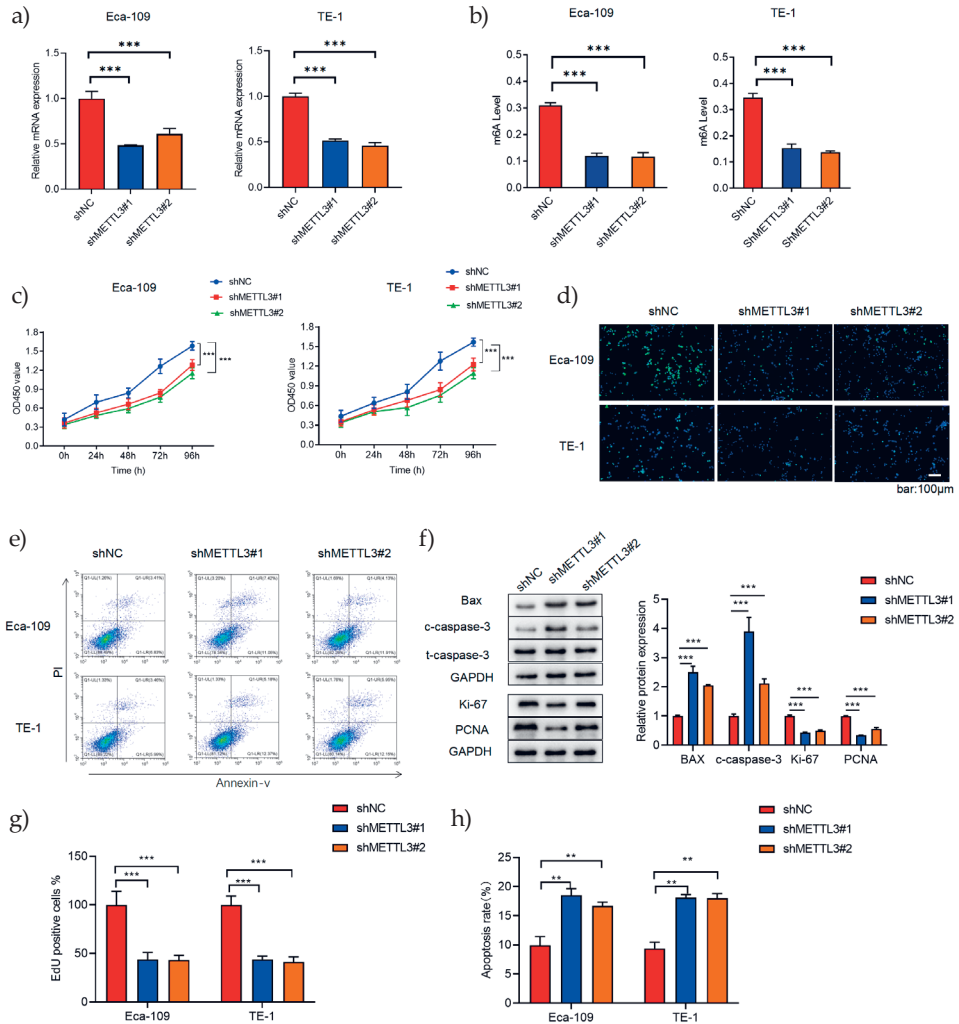


Fig. 2. METTL3 silencing suppressed proliferation and accelerated apoptosis of EC cells: a) mRNA expression of METTL3 in Eca-109 and TE-1 cells treated with shNC, shMETTL3-1, and shMETTL3-2 to confirm transfection efficiency by qRT-PCR; b) m6A RNA methylation was estimated using a colorimetric method; c) cell proliferation of transfected Eca-109 and TE-1 cells assessed by performing a CCK-8 experiment; d) EdU incorporation assay in Eca-109 and TE-1 cells; e) Apoptosis of Eca-109 and TE-1 cells was tested by flow cytometry. (F) Bax, c-caspase-3, t-caspase-3, Ki67, and PCNA proteins are expressed in Eca-109 cells with or without shMETTL3; g) and h) quantified data of EdU incorporation assay and flow cytometry. * $p < 0.05$, ** $p < 0.01$, *** $p < 0.001$.

(Eca-109: shNC vs. shMETTL3-1, $p < 0.001$; shNC vs. shMETTL3-2, $p < 0.001$) (TE-1: shNC vs. shMETTL3-1, $p < 0.001$; shNC vs. shMETTL3-2, $p < 0.001$). The CCK-8 assay demonstrated that METTL3 downregulation inhibited cell proliferation (Fig. 2c) (Eca-109: shNC vs. sh

METTL3-1, $p < 0.001$; shNC *vs.* sh*METTL3-2*, $p < 0.001$) (TE-1: shNC *vs.* sh*METTL3-1*, $p < 0.001$; shNC *vs.* sh*METTL3-2*, $p < 0.001$). The EdU assay showed a decrease in the abundance of proliferating cells when *METTL3* expression was downregulated (Fig. 2d,g) (Eca-109: shNC *vs.* sh*METTL3-1*, $p < 0.001$; shNC *vs.* sh*METTL3-2*, $p < 0.001$) (TE-1: shNC *vs.* sh*METTL3-1*, $p < 0.001$; shNC *vs.* sh*METTL3-2*, $p < 0.001$). Flow cytometry analysis revealed an increase in apoptotic cells following *METTL3* knockdown (Fig. 2e,h) (Eca-109: shNC *vs.* sh*METTL3-1*, $p = 0.009$; shNC *vs.* sh*METTL3-2*, $p = 0.008$) (TE-1: shNC *vs.* sh*METTL3-1*, $p = 0.007$; shNC *vs.* sh*METTL3-2*, $p = 0.008$). WB analysis showed that the expression levels of the proapoptotic proteins Bax and c-caspase-3 increased after *METTL3* knockdown, while there was no significant change in t-caspase-3 levels. Additionally, the levels of proliferation-related proteins Ki-67 and PCNA decreased compared to the control group (Fig. 2f) (BAX: shNC *vs.* sh*METTL3-1*, $p < 0.001$; shNC *vs.* sh*METTL3-2*, $p < 0.001$) (c-caspase-3: shNC *vs.* sh*METTL3-1*, $p < 0.001$; shNC *vs.* sh*METTL3-2*, $p < 0.001$) (Ki-67: shNC *vs.* sh*METTL3-1*, $p < 0.001$; shNC *vs.* sh*METTL3-2*, $p < 0.001$) (PCNA: shNC *vs.* sh*METTL3-1*, $p < 0.001$; shNC *vs.* sh*METTL3-2*, $p < 0.001$). These findings illustrate that *METTL3* inhibition impedes proliferation while inducing apoptosis in EC.

METTL3 regulated the m6A modification of FOXD2-AS1

SRAMP predicted 12 m6A-modified sites (Fig. 3a). Several of the analyzed binding sites showed above moderate confidence. MeRIP assays revealed that the m6A level in

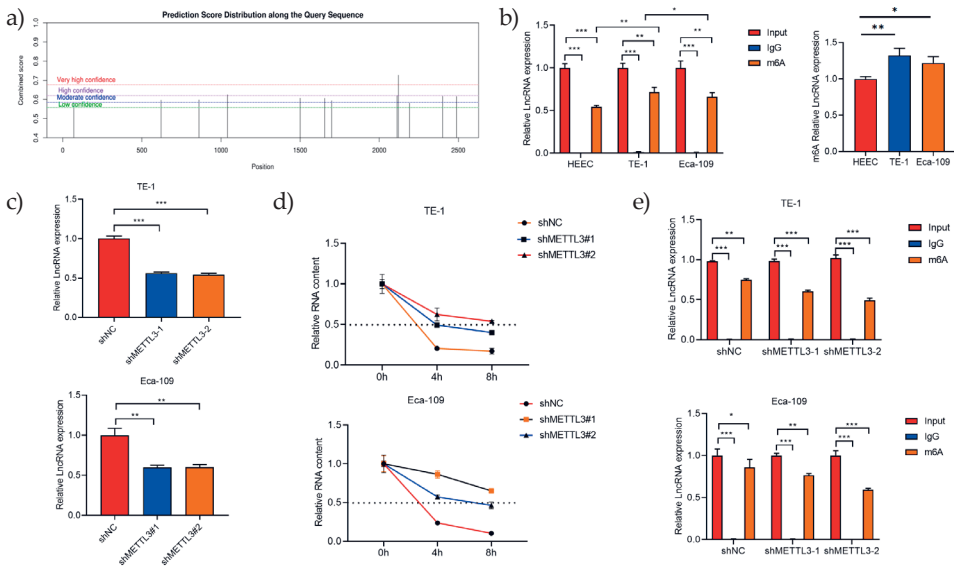


Fig. 3 *METTL3* regulated the m6A modification of FOXD2-AS1: a) analysis of m6A-modified sites in FOXD2-AS1 by SRAMP; b) MeRIP-qPCR analysis of m6A levels in HEEC, TE-1, and Eca-109 cells; c) qRT-PCR results showing the expression of FOXD2-AS1 after transfection with shNC, sh*METTL3-1*, and sh*METTL3-2*; d) evaluation of FOXD2-AS1 RNA stability in TE-1 and Eca-109 cells with or without *METTL3* shRNA; e) MeRIP-qPCR analysis of m6A levels following *METTL3* silencing in TE-1 and Eca-109 cells. * $p < 0.05$, ** $p < 0.01$, *** $p < 0.001$.

Eca-109 and TE-1 cells was higher than that in HEEC cells (Fig. 3b) (HEEC: Input *vs.* IgG, $p < 0.001$; Input *vs.* m6A, $p < 0.001$) (Eca-109: Input *vs.* IgG, $p < 0.001$; Input *vs.* m6A, $p = 0.007$) (TE-1: Input *vs.* IgG, $p < 0.001$; Input *vs.* m6A, $p = 0.006$) (m6A content: HEEC cells *vs.* TE-1 cells, $p = 0.006$; HEEC cells *vs.* Eca-109 cells, $p = 0.017$). During qRT-PCR experiments, *FOXD2-AS1* expression was significantly reduced upon METTL3 inhibition (Fig. 3c) (Eca-109: shNC *vs.* shMETTL3-1, $p < 0.001$; shNC *vs.* shMETTL3-2, $p < 0.001$) (TE-1: shNC *vs.* shMETTL3-1, $p < 0.001$; shNC *vs.* shMETTL3-2, $p < 0.001$). Subsequently, the effect of *METTL3* knockdown on the stability of *FOXD2-AS1* was investigated, revealing that *METTL3* knockdown improved the stability of *FOXD2-AS1* RNA in Eca-109 and TE-1 cells (Fig. 3d) (Eca-109: 4h- shNC *vs.* shMETTL3-1, $p < 0.001$; shNC *vs.* shMETTL3-2, $p = 0.0002$; 8h- shNC *vs.* shMETTL3-1, $p < 0.001$; shNC *vs.* shMETTL3-2, $p = 0.010$) (TE-1: 4h- shNC *vs.* shMETTL3-1, $p < 0.001$; shNC *vs.* shMETTL3-2, $p = 0.023$; 8h- shNC *vs.* shMETTL3-1, $p = 0.008$; shNC *vs.* shMETTL3-2, $p = 0.004$). Moreover, *METTL3* silencing decreased the m6A level in Eca-109 and TE-1 cells (Fig. 3e) (Eca-109: sh-NC- Input *vs.* IgG, $p < 0.001$; Input *vs.* m6A, $p = 0.043$; shMETTL3-1- Input *vs.* IgG, $p < 0.001$; Input *vs.* m6A, $p = 0.009$; shMETTL3-2- Input *vs.* IgG, $p < 0.001$; Input *vs.* m6A, $p = 0.008$) (TE-1: shNC- Input *vs.* IgG, $p < 0.001$; Input *vs.* m6A, $p = 0.007$; shMETTL3-1- Input *vs.* IgG, $p < 0.001$; Input *vs.* m6A, $p = 0.0004$; shMETTL3-2- Input *vs.* IgG, $p < 0.001$; Input *vs.* m6A, $p < 0.001$). These results clarify that METTL3 modulates the m6A modification of *FOXD2-AS1* in EC.

YTHDF1 bound with FOXD2-AS1

To identify the functional proteins involved in the m6A modification of *FOXD2-AS1*, RIP experiments were conducted. YTHDF1, YTHDF2, and YTHDF3 were found to bind with *FOXD2-AS1*, with YTHDF1 exhibiting the highest affinity (Fig. 4a-c) (Eca-109: IgG *vs.* YTHDF1, $p < 0.001$; TE-1-IgG *vs.* YTHDF1, $p < 0.001$) (Eca-109: IgG *vs.* YTHDF2, $p < 0.001$; TE-1-IgG *vs.* YTHDF2, $p < 0.001$) (Eca-109: IgG *vs.* YTHDF3, $p < 0.001$; TE-1-IgG *vs.* YTHDF3, $p < 0.001$). The positive correlation between YTHDF1 and *FOXD2-AS1* in EC was analyzed by GEPIA (Pearson correlation coefficient) ($R = 0.38$, $p < 0.001$) (Fig. 4d). RNA pull-down experiments validated the interaction between the YTHDF1 protein and *FOXD2-AS1* (Fig. 4e). Subsequently, YTHDF1 was either upregulated or downregulated, and the transfection efficacy was confirmed by western blot (Fig. 4f,g) (Fig. 4 F: Eca-109: shNC *vs.* shMETTL3-1, $p < 0.001$; TE-1: shNC *vs.* shMETTL3-1, $p < 0.001$) (Fig. 4g: Eca-109: Vector *vs.* YTHDF1, $p = 0.006$; TE-1: Vector *vs.* YTHDF1, $p = 0.005$) *FOXD2-AS1* expression was significantly increased or decreased after YTHDF1 overexpression or knockdown, as assessed by qRT-PCR (Fig. 4h) (Eca-109: shNC *vs.* shYTHDF1, $p < 0.001$; Vector *vs.* YTHDF1, $p = 0.005$; TE-1: shNC *vs.* shYTHDF1, $p < 0.001$; Vector *vs.* YTHDF1, $p < 0.001$). Co-IP experiments confirmed the interaction between METTL3 protein and YTHDF1 protein (Fig. 4i). Moreover, RIP experiments confirmed that the interaction between YTHDF1 and *FOXD2-AS1* was modulated when *METTL3* expression was downregulated or upregulated (Fig. 4j) (Left: Eca-109: IgG: Vector *vs.* *METTL3*, $p = 0.767$; YTHDF1: Vector *vs.* *METTL3*, $p = 0.006$; TE-1: IgG: Vector *vs.* *METTL3*, $p = 0.835$; YTHDF1: Vector *vs.* *METTL3*, $p = 0.004$) (Right: Eca-109: IgG: shNC *vs.* shMETTL3, $p = 0.713$; YTHDF1: shNC *vs.* shMETTL3, $p < 0.001$; TE-1: IgG: shNC *vs.* shMETTL3, $p = 0.849$; YTHDF1: shNC *vs.* shMETTL3, $p = 0.037$). These results collectively demonstrate that METTL3 regulates the interaction between YTHDF1 and *FOXD2-AS1*.

METTL3 regulated FOXD2-AS1 m6A modification to affect EC in vivo

Animal models were categorized into the NC group, METTL3 KD group, FOXD2-AS1 OE group, and METTL3 KD+FOXD2-AS1 OE group. Tumor sizes and volumes were significantly smaller in the METTL3 KD group than in the NC group, while larger tumor sizes and volumes were observed in the FOXD2-AS1 OE group. Tumor sizes and volumes were

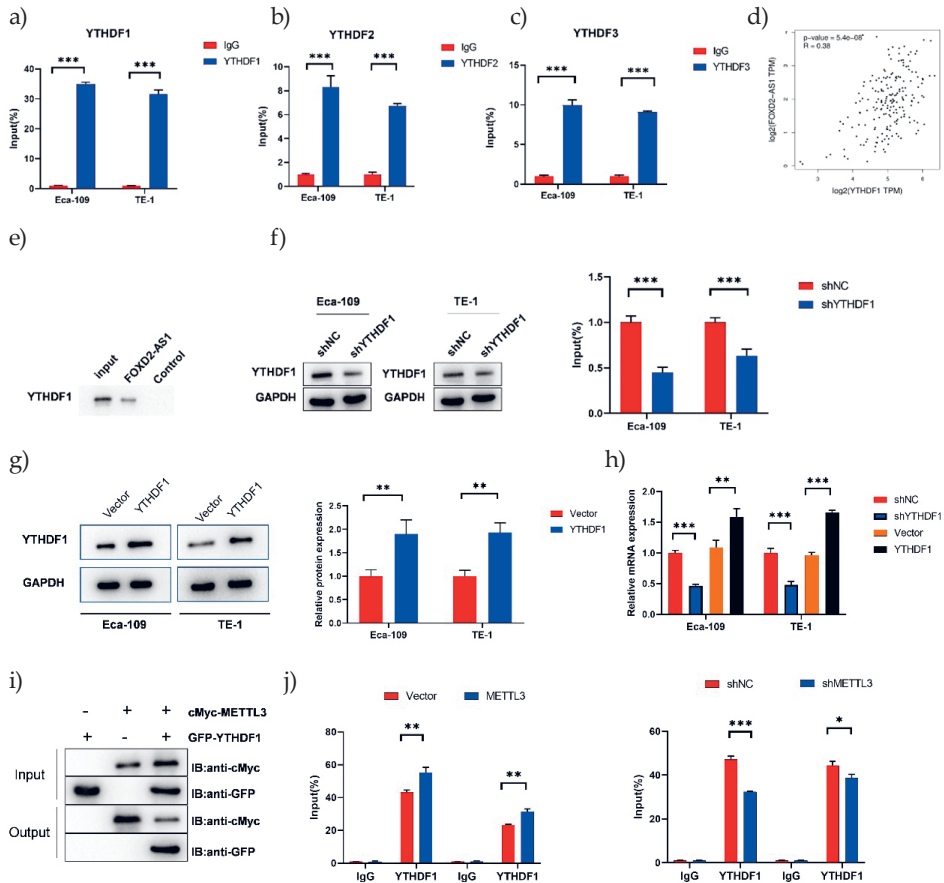


Fig. 4. YTHDF1 interaction with FOXD2-AS1: a) to c) RIP assay measured the binding affinity of FOXD2-AS1 with m6A methylation-reading proteins YTHDF1, YTHDF2, and YTHDF3; d) GEPIA analyzed a positive correlation between FOXD2-AS1 and YTHDF1 in EC; e) RNA pull-down analysis determined the binding of FOXD2-AS1 with YTHDF1; f) to h) tumor cells were transfected with shNC, shYTHDF1, vector, and YTHDF1, and their effects were assessed by western blot. Changes in *FOXDF2-AS1* expression following YTHDF1 downregulation or upregulation were explored using qRT-PCR; i) CO-IP assay probed the interaction between METTL3 and YTHDF1; j) RIP assay investigated the effects of *METTL3* knockdown or upregulation on the interaction between FOXD2-AS1 and YTHDF1. The impact of METTL3 depletion on their binding was also estimated through RIP assay. * $p < 0.05$, ** $p < 0.01$, *** $p < 0.001$.

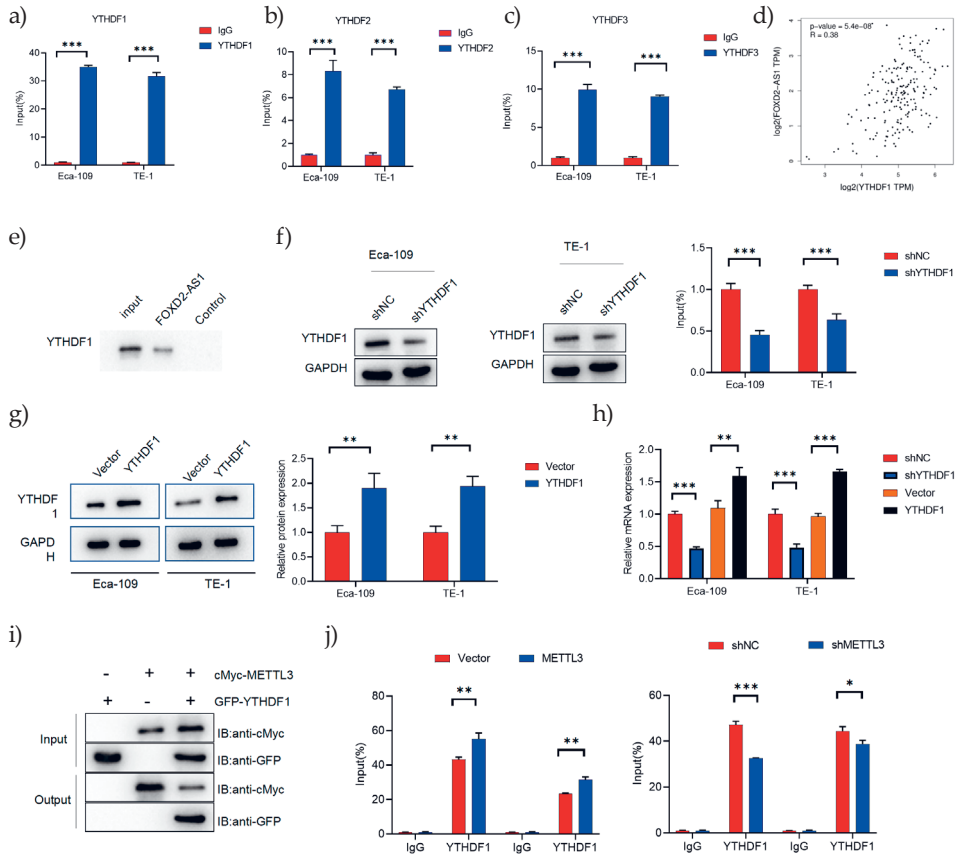


Fig. 4. Continued.

significantly larger in the FOXD2-AS1 OE group compared to the METTL3 KD group (Fig. 5a,b) (Fig. 5b: NC vs. METTL3 KD, $p < 0.001$; NC vs. FOXD2-AS1 OE, $p < 0.001$; METTL3 KD vs. METTL3 KD+FOXD2-AS1 OE, $p = 0.004$; METTL3 KD+FOXD2-AS1 OE vs. FOXD2-AS1 OE, $p < 0.001$) (Fig. 5c: NC vs. METTL3 KD, $p < 0.001$; NC vs. FOXD2-AS1 OE, $p = 0.048$; METTL3 KD vs. METTL3 KD+FOXD2-AS1 OE, $p = 0.005$; METTL3 KD+FOXD2-AS1 OE vs. FOXD2-AS1 OE, $p = 0.049$). Additionally, tumor weights were significantly reduced with METTL3 silencing but markedly increased with FOXD2-AS1 overexpression. Furthermore, tumor weights in the METTL3 KD+FOXD2-AS1 OE group were significantly heavier compared to the METTL3 KD group (Fig. 5c) (NC vs. METTL3 KD, $p = 0.005$; NC vs. FOXD2-AS1 OE, $p = 0.527$; METTL3 KD vs. METTL3 KD+FOXD2-AS1 OE, $p = 0.298$; METTL3 KD+FOXD2-AS1 OE vs. FOXD2-AS1 OE, $p = 0.005$). qRT-PCR analysis of tissues indicated that FOXD2-AS1 expression was decreased after METTL3 knockdown but enhanced following FOXD2-AS1 overexpression vector transfection. Moreover, the decrease in FOXD2-AS1 due to METTL3 silencing was reversed by FOXD2-AS1 overexpression vector transfection (Fig. 5d-e) (NC vs. METTL3 KD, $p < 0.001$; NC vs. FOXD2-AS1 OE, $p = 0.005$;

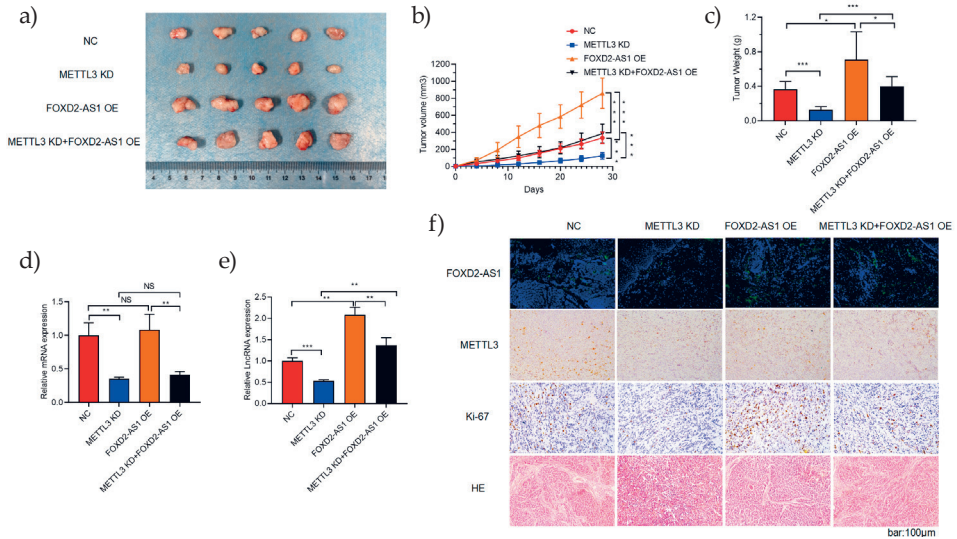


Fig. 5. METTL3 regulated FOXD2-AS1 m6A modification to affect EC *in vivo*. Animals were divided into the NC group, METTL3 KD group, FOXD2-AS1 OE group, and METTL3 KD+FOXD2-AS1 OE group. a) pictures of tumors were exhibited; b) tumor volumes were measured every third day; c) tumor weights were recorded and plotted as a histogram; d) qRT-PCR analysis of the METTL3 expression in tissues of four groups; e) qRT-PCR analysis of the FOXD2-AS1 expression in tissues of four groups; f) representative images of FISH staining for FOXD2-AS1, immunohistochemical staining for METTL3 and Ki-67, and HE staining of the tumors of mice. * $p < 0.05$, ** $p < 0.01$, *** $p < 0.001$.

METTL3 KD vs. METTL3 KD+FOXD2-AS1 OE, $p = 0.007$; METTL3 KD+FOXD2-AS1 OE vs. FOXD2-AS1 OE, $p = 0.006$). Upregulation of FOXD2-AS1 abrogated the mitigation of tissue injury caused by METTL3 silencing. FISH experiments revealed FOXD2-AS1 expression in tumor tissue, confirming that FOXD2-AS1 expression was reduced after METTL3 knockdown but enhanced after FOXD2-AS1 overexpression vector transfection. Immunohistochemistry revealed the expression levels of METTL3 and Ki67 in tumor tissues, with METTL3 knockdown reversing the upregulation of Ki67 levels caused by FOXD2-AS1 overexpression. However, METTL3 expression in the METTL3 KD group was downregulated, while METTL3 expression in other groups remained unchanged (Fig. 5f). Thus, METTL3 mediated FOXD2-AS1 m6A modification to affect EC *in vivo*.

FOXD2-AS1, recognized for its role as an oncogene in esophageal cancer (EC), has been implicated in several aspects of the disease. For instance, Xue *et al.* demonstrated that FOXD2-AS1, in collaboration with MACC1-AS1, mediates cisplatin resistance in ESCC cells through NSD2 (15). Liu *et al.* revealed that FOXD2-AS1 overexpression induces cisplatin resistance in ESCC by interacting with miR-195 to regulate the Akt/mTOR pathway (16). Additionally, our previous work has demonstrated that FOXD2-AS1 enhances the proliferation and invasion capacities of EC cells *via* the miR-145-5p/CDK6 axis (17). Based on these findings, we systematically explored the mechanisms regulating FOXD2-AS1 in EC.

Extensive research has revealed the critical involvement of dysregulated m6A RNA methylation in various cancers, where it can exert either enhancing or suppressive effects

(37, 38). Furthermore, emerging evidence suggests that long non-coding RNAs play a role in modulating METTL3 in various carcinomas. For example, in non-small-cell lung cancer, METTL3 promotes ABHD11-AS1 expression to enhance the Warburg effect (39). METTL3 has also been shown to stabilize the lncRNA SNHG7, thereby regulating the SRSF1/c-Myc axis and accelerating glycolysis in prostate cancer (40). Notably, we identified 12 m6A-mediated sites on *FOXD2-AS1* using SRAMP, suggesting METTL3's involvement in the regulation of *FOXD2-AS1*. Moreover, predictions from the ENCORI database indicate that only *METTL3*, not *METTL14*, exhibits relatively high expression in EC. Consistently, we observed upregulation of METTL3 expression in EC tissues and cells compared to normal counterparts. Subsequent functional experiments revealed that inhibition of METTL3 impedes proliferation and induces apoptosis in Eca-109 and TE-1 cells. These results suggest that *METTL3* may regulate EC proliferation and apoptosis. Additionally, MeRIP assays confirmed a high m6A level on *FOXD2-AS1*, which was decreased when *METTL3* expression was silenced, suggesting that *FOXD2-AS1* might be mediated by METTL3 in an m6A-dependent manner.

Previous research has highlighted the crucial roles of m6A readers in facilitating the processing of m6A RNA methylation. For example, Anita *et al.* found that the dysregulation of m6A readers YTHDF1 and YTHDF3 is associated with metastasis and prognosis in breast cancer patients (41). In liver cancer, YTHDF2 was shown to facilitate the stem cell phenotype and metastasis by influencing OCT4 levels (42). To uncover the m6A reader involved in the modulation of *FOXD2-AS1* by METTL3, we conducted RIP assays to measure the binding affinity between YTHDF1, YTHDF2, or YTHDF3 with *FOXD2-AS1*. Our results revealed the highest binding affinity between YTHDF1 and *FOXD2-AS1*, and this positive correlation was further supported by predictions from the GEPIA database. Subsequent mechanistic assays confirmed that METTL3 could influence the binding of YTHDF1 to *FOXD2-AS1*. Moreover, *in vivo* assays, we demonstrated that METTL3 regulates *FOXD2-AS1* to control EC tumor growth. This study represents the first exploration of m6A RNA methylation in EC and the mechanism underlying the METTL3/YTHDF1/*FOXD2-AS1* axis in EC.

CONCLUSIONS

Our findings suggest that METTL3 regulates *FOXD2-AS1* in an m6A-dependent manner through its interaction with YTHDF1, ultimately mediating the proliferation and apoptosis abilities of EC cells. These discoveries provide valuable insights into potential therapeutic targets for the treatment of EC patients.

Conflicts of interest. – The authors declare no conflict of interest.

Funding. – This project was supported by Jiangsu Provincial Health Commission Research Project Approval (No:M2021089).

Authors contributions. – Conceptualization, W.C.W.; investigation, X.C.L., statistical analysis, Z.Y.G., graphics, W.D.S.; writing, original draft preparation, review, and editing, Z.J.W. All authors have read and agreed to the published version of the manuscript.

REFERENCES

1. K. Liu, T. Zhao, J. Wang, Y. Chen, R. Zhang, X. Lan and J. Que, Etiology, cancer stem cells and potential diagnostic biomarkers for esophageal cancer, *Cancer Lett.* **458**(28) (2019) 21–28; <https://doi.org/10.1016/j.canlet.2019.05.018>
2. Y. Baba, D. Nomoto, K. Okadome, T. Ishimoto, M. Iwatsuki, Y. Miyamoto, N. Yoshida and H. Baba, Tumor immune microenvironment and immune checkpoint inhibitors in esophageal squamous cell carcinoma, *Cancer Sci.* **111**(9) (2020) 3132–3141; <https://doi.org/10.1111/cas.14541>
3. K. Harada, J. E. Rogers, M. Iwatsuki, K. Yamashita, H. Baba and J. A. Ajani, Recent advances in treating oesophageal cancer, *F1000. Res.* **10**(1) (2020) 1180–11891; <https://doi.org/10.12688/f1000research.22926.1>
4. T. M. Godefa, S. Derks and V. L. J. L. Thijssen, Galectins in esophageal cancer: Current knowledge and future perspectives, *Cancers* (Basel) **14**(23) (2022) Article ID 5790; <https://doi.org/10.3390/cancers14235790>
5. P. Thuss-Patience and S. Stein, Immunotherapy in squamous cell cancer of the esophagus, *Curr. Oncol.* **29**(4) (2022) 2461–2471; <https://doi.org/10.3390/curroncol29040200>
6. K. Kato, Y. Ito, I. Nozaki, H. Daiko, T. Kojima, M. Yano, M. Ueno, S. Nakagawa, M. Takagi, S. Tsunoda, T. Abe, T. Nakamura, M. Okada, Y. Toh, Y. Shibuya, S. Yamamoto, H. Katayama, K. Nakamura and Y. Kitagawa, Japan Esophageal Oncology Group of the Japan Clinical Oncology Group, Parallel-group controlled trial of surgery versus chemoradiotherapy in patients with stage I esophageal squamous cell carcinoma, *Gastroenterology* **161**(6) (2021) 1878–1886; <https://doi.org/10.1053/j.gastro.2021.08.007>
7. R. Li, L. Zeng, H. Zhao, J. Deng, L. Pan, S. Zhang, G. Wu, Y. Ye, J. Zhang, J. Su, Y. Zheng, S. Deng, R. Bai, L. Zhuang, M. Li, Z. Zuo, D. Lin, J. Zheng and X. Huang, ATXN2-mediated translation of TNFR1 promotes esophageal squamous cell carcinoma via m⁶A-dependent manner, *Mol. Ther.* **30**(3) (2022) 1089–1103; <https://doi.org/10.1016/j.ymt.2022.01.006>
8. J. Xu, W. Cao, A. Shao, M. Yang, V. Andoh, Q. Ge, H. W. Pan and K. P. Chen, Metabolomics of esophageal squamous cell carcinoma tissues: Potential biomarkers for diagnosis and promising targets for therapy, *Biomed. Res. Int.* **23** (2022) Article ID 7819235 (24 pages); <https://doi.org/10.1155/2022/7819235>
9. J. Venkatesh, M. D. Wasson, J. M. Brown, W. Fernando and P. Marcato, LncRNA-miRNA axes in breast cancer: Novel points of interaction for strategic attack, *Cancer Lett.* **509**(1) (2021) 81–88; <https://doi.org/10.1016/j.canlet.2021.04.002>
10. Y. Chi, D. Wang, J. Wang, W. Yu and J. Yang, Long non-coding RNA in the pathogenesis of cancers, *Cells* **8**(9) (2021) 1015; <https://doi.org/10.3390/cells8091015>
11. Y. Lan, B. Liu and H. Guo, The role of m⁶A modification in the regulation of tumor-related lncRNAs, *Mol. Ther. Nucleic Acids* **24** (2021) 768–779; <https://doi.org/10.1016/j.omtn.2021.04.002>
12. L. Chen, C. H. Qiu, Y. Chen, Y. Wang, J. J. Zhao and M. Zhang, LncRNA SNHG16 drives proliferation, migration, and invasion of lung cancer cell through modulation of miR-520/VEGF axis, *Eur. Rev. Med. Pharmacol.* **24**(18) (2020) 9522–9531; https://doi.org/10.26355/eurev_202009_23037
13. X. Chen, Y. Liu, D. Sun, R. Sun, X. Wang, M. Li, N. Song, J. Ying, T. Guo and Y. Jiang, Long noncoding RNA lnc-H2AFV-1 promotes cell growth by regulating aberrant m⁶A RNA modification in head and neck squamous cell carcinoma, *Cancer Sci.* **113**(6) (2022) 2071–2084; <https://doi.org/10.1111/CAS.15366>
14. B. Xiu, Y. Chi, L. Liu, W. Chi, Q. Zhang, J. Chen, R. Guo, J. Si, L. Li, J. Xue, Z. M. Shao, Z. H. Wu, S. Huang and J. Wu, LINC02273 drives breast cancer metastasis by epigenetically increasing AGR2 transcription, *Mol. Cancer* **18**(1) (2019) Article ID 187 (20 pages); <https://doi.org/10.1186/s12943-019-1115-y>
15. W. Xue, Z. Shen, L. Li, Y. Zheng, D. Yan, Q. Kan and J. Zhao, Long non-coding RNAs MACC1-AS1 and FOXD2-AS1 mediate NSD2-induced cisplatin resistance in esophageal squamous cell carcinoma, *Mol. Ther. Nucleic Acids* **10**(23) (2020) 592–602; <https://doi.org/10.1016/j.omtn.2020.12.007>

16. H. Liu, J. Zhang, X. Luo, M. Zeng, L. Xu, Q. Zhang, H. Liu, J. Guo and L. Xu, Overexpression of the long noncoding RNA FOXD2-AS1 promotes cisplatin resistance in esophageal squamous cell carcinoma through the miR-195/Akt/mTOR axis, *Oncol. Res.* 28(1) (2020) 65–73; <https://doi.org/10.3727/096504019X15656904013079>
17. W. Shi, Z. Gao, J. Song and W. Wang, Silence of FOXD2-AS1 inhibited the proliferation and invasion of esophagus cells by regulating miR-145-5p/CDK6 axis, *Histol. Histopathol.* 35(9) (2020) 1013–1021; <https://doi.org/10.14670/HH-18-232>
18. T. Sun, R. Wu and L. Ming, The role of m6A RNA methylation in cancer, *Biomed. Pharmacother.* 4(112) (2019) Article ID 108613 (9 pages); <https://doi.org/10.1016/j.biopha.2019.108613>
19. S. Ma, C. Chen, X. Ji, J. Liu, Q. Zhou, G. Wang, W. Yuan, Q. Kan and Z. Sun, The interplay between m6A RNA methylation and noncoding RNA in cancer, *J. Hematol. Oncol.* 12(1) (2019) Article ID 121 (15 pages); <https://doi.org/10.1186/s13045-019-0805-7>
20. L. Rowe and A. L. Rockwell, Ubiquitous knockdown of *Mettl3* using TRiP.GL01126 results in spermatid mislocalization during *Drosophila* spermatogenesis, *MicroPubl. Biol.* 17(18) (2022) 17912–17918; <https://doi.org/10.17912/micropub.biology.000511>
21. K. I. Zhou and T. Pan, Structures of the m(6) A methyltransferase complex: Two subunits with distinct but coordinated roles, *Mol. Cell* 63(2) (2016) 183–185; <https://doi.org/10.1016/j.molcel.2016.07.005>
22. H. Zhou, K. Yin, Y. Zhang, J. Tian and S. Wang, The RNA m6A writer METTL14 in cancers: Roles, structures, and applications, *Biochim. Biophys. Acta. Rev. Cancer* 1876(2) (2021) Article ID 188609; <https://doi.org/10.1016/j.bbcan.2021.188609>
23. Z. Chen, X. Zhong, M. Xia and J. Zhong, The roles and mechanisms of the m6A reader protein YTHDF1 in tumor biology and human diseases, *Mol. Ther. Nucleic Acids* 26(9) (2021) 1270–1279; <https://doi.org/10.1016/J.OMTN.2021.10.023>
24. S. Li, F. Jiang, F. Chen, Y. Deng and X. Pan, Effect of m6A methyltransferase METTL3-mediated MALAT1/E2F1/AGR2 axis on adriamycin resistance in breast cancer, *J. Biochem. Mol. Toxicol.* 36 (2022) Article ID e22922 (12 pages); <https://doi.org/10.1002/jbt.22922>
25. H. Chen, Y. Yu, M. Yang, H. Huang, S. Ma, J. Hu, Z. Xi, H. Guo, G. Yao, L. Yang, X. Huang, F. Zhang, G. Tan, H. Wu, W. Zheng and L. Li, YTHDF1 promotes breast cancer progression by facilitating FOXM1 translation in an m6A-dependent manner, *Cell Biosci.* 12(1) (2022) Article ID 19 (16 pages); <https://doi.org/10.1186/S13578-022-00759-w>
26. J.-H. Li, S. Liu, H. Zhou, L.-H. Qu and J. H. Yang, Starbase v2.0: Decoding miRNA-ceRNA, miRNA-ncRNA and protein-RNA interaction networks from large-scale CLIP-Seq data, *Nucleic Acids Res.* 42(D1) (2014) D92–D97; <https://doi.org/10.1093/nar/gkt1248>
27. D. S. Chandrashekar, S. K. Karthikeyan, P. K. Korla, H. Patel, A. R. Shovon, M. Athar, G. J. Netto, Z. S. Qin, S. Kumar, U. Manne, C. J. Creighton and S. Varambally, UALCAN: An update to the integrated cancer data analysis platform, *Neoplasia* 25 (2022) 18–27; <https://doi.org/10.1016/j.neo.2022.01.001>
28. D. S. Chandrashekar, B. Bashel, S. A. H. Balasubramanya, C. J. Creighton, I. Ponce-Rodriguez, V. S. K. Chakravarthi and S. Varambally, UALCAN: A Portal for facilitating tumor subgroup gene expression and survival analyses, *Neoplasia* 19(8) (2017) 649–658; <https://doi.org/10.1016/j.neo.2017.05.002>
29. Y. Zhou, P. Zeng, Y. H. Li, Z. Zhang and Q. Cui, SRAMP: Prediction of mammalian N6-methyladenosine (m6A) sites based on sequence-derived features, *Nucleic Acids Res.* 44(10) (2016) Article ID e91; <https://doi.org/10.1093/nar/gkw104>
30. R. Fan, C. Cui, B. Kang, Z. Chang, G. Wang and Q. Cui, A combined deep learning framework for mammalian m6A site prediction, *Cell Genomic* 4(12) (2024) Article ID 100697 (13 pages); <https://doi.org/10.1016/j.xgen.2024.100697>
31. Z. Tang, C. Li, B. Kang, G. Gao, C. Li and Z. Zhang, GEPIA: A web server for cancer and normal gene expression profiling and interactive analyses, *Nucleic Acids Res.* 45(W1) (2017) W98–W102; <https://doi.org/10.1093/nar/gkx247>
32. The Cancer Genome Atlas Research Network. Integrated genomic characterization of oesophageal carcinoma, *Nature* 541(7636) (2017) 169–175; <https://doi.org/10.1038/nature20805>

33. K. J. Livak and T. D. Schmittgen, Analysis of relative gene expression data using real-time quantitative PCR and the $2^{-\Delta\Delta CT}$ method, *Methods* 25(4) (2001) 402–408; <https://doi.org/10.1006/meth.2001.1262>
34. J. Ye, G. Coulouris, I. Zaretskaya, I. Cutcutache, S. Rozen and T. L. Madden, Primer-BLAST: A tool to design target-specific primers for polymerase chain reaction, *BMC Bioinformatics* 13 (2012) Article 134 (11 pages); <https://doi.org/10.1186/1471-2105-13-134>
35. C. A. Schneider, W. S. Rasband and K. W. Eliceiri, NIH Image to ImageJ: 25 years of image analysis, *Nat. Methods* 9(7) (2012) 671–675; <https://doi.org/10.1038/nmeth.2089>
36. J. Cai, Z. Chen, J. Wang, X. Chen, L. Liang, M. Huang, Z. Zhang and X. Zuo, circHECTD1 facilitates glutaminolysis to promote gastric cancer progression by targeting miR-1256 and activating β -catenin/c-Myc signaling, *Cell Death Dis.* 10(8) (2019) Article ID 576 (15 pages); <https://doi.org/10.1038/s41419-019-1814-8>
37. X.-Y. Chen, J. Zhang and J.-S. Zhu, The role of m⁶A RNA methylation in human cancer, *Mol. Cancer* 18(1) (2019) Article ID 103 (9 pages); <https://doi.org/10.1186/s12943-019-1033-z>
38. C. Zhang, J.-H. Liu, H. Guo, D. Hong, J. Ji, Q. Zhang, Q. Guan and Q. Ren, m⁶A RNA methylation regulators were associated with the malignancy and prognosis of ovarian cancer, *Bioengineered* 12(1) (2021) 3159–3176; <https://doi.org/10.1080/21655979.2021.1946305>
39. L. Xue, J. Li, Y. Lin, D. Liu, Q. Yang, J. Jian and J. Peng, m⁶A transferase METTL3-induced lncRNA ABHD11-AS1 promotes the Warburg effect of non-small-cell lung cancer, *J. Cell Physiol.* 236(4) (2012) 2649–2658; <https://doi.org/10.1002/jcp.30023>
40. L. Liu, J.-F. Yuan and Y.-Z. Wang, METTL3-stabilized lncRNA SNHG7 accelerates glycolysis in prostate cancer via SRSF1/c-Myc axis, *Exp. Cell Res.* 416(1) (2022) Article ID 113149; <https://doi.org/10.1016/j.yexcr.2022.113149>
41. R. Anita, A. Paramasivam, J. V. Priyadharsini and S. Chitra, The m⁶A readers YTHDF1 and YTHDF3 aberrations associated with metastasis and predict poor prognosis in breast cancer patients, *Am. J. Cancer Res.* 10(8) (2020) 2546–2554.
42. C. Zhang, S. Huang, H. Zhuang, S. Ruan, Z. Zhou, K. Huang, F. Ji, Z. Ma, B. Hou and X. He, YTHDF2 promotes the liver cancer stem cell phenotype and cancer metastasis by regulating OCT4 expression via m⁶A RNA methylation, *Oncogene* 39(23) (2020) 4507–4518; <https://doi.org/10.1038/s41388-020-1303-7>